Numerical and experimental investigation of an atmospheric pressure DC corona discharge

G. Mongaretto[1], F. Ragazzi[1], G. Neretti[1], G. Caliò[2], A. Popoli[1], G. Pierotti[1], A. Cristofolini[1], L. Valdettaro [2], P. Barbante [2], C. De Falco [2]

[1] *Department of Electrical, Electronic and Information Engineering "Guglielmo Marconi", University of Bologna, Bologna, Italy*

[2] *MOX – Modelling and Scientific Computing, Department of Mathematics, Politecnico di Milano, Milan, Italy*

Introduction

In recent years, plasma-based propulsion has gained considerable attention, particularly for space applications where it is now an established technology [1]. More recently, interest has started to grow towards extending similar concepts for operation in atmospheric conditions [2]. In this context, electrohydrodynamic (EHD) thrusters based on corona discharges are promising, generating thrust through momentum exchange between ions and neutral gas, producing what is known as ionic wind. These devices are typically modeled with two regions: the ionization region, where a strong electric field creates charge carriers, and the drift region, where ions accelerate and transfer momentum to neutrals. Accurate modeling of these processes is essential for improving the performance and efficiency of atmospheric plasma propulsion systems. In this paper, we present the results predicted by a 1D *drift-diffusion-reaction* model applied to a concentric wire-cylinder geometry at atmospheric pressure. Furthermore, the predictions from the numerical model are compared with experimental data obtained from a measurement campaign conducted on a reactor with the same geometry, showing good agreement.

Physical and numerical model

The physical model consists of the continuity equations for the considered species, formulated within the *drift-diffusion* approximation [3], coupled with Poisson's equation:

$$\frac{\partial n_s}{\partial t} + \nabla \cdot [-D_s \nabla n_s - sign(q_s)\mu_s n_s \nabla \varphi] = \Omega_s. \tag{1}$$

Here n_s is the number density of species s, Ω_s is the source term due to chemical reactions, D_s and μ_s are the diffusion coefficient and the mobility and φ is the electric scalar potential. The model is based on a reference geometry consisting of a concentric wire-cylinder arrangement, resulting in a one-dimensional computational domain. This domain is discretized using a hyperbolic-tangent mesh, and the governing equations are solved with a finite volume

method (FVM). Specifically, for the continuity equation, a second-order centered finite difference scheme is applied to the diffusive term, while a first-order upwind scheme is used for the advective drift term as in [3]. The source term Ω_s in (1) is computed using three different reduced kinetic models for dry air, all under the local field approximation and assuming constant ion and neutral gas temperatures at 300 K. The first chemical scheme is a simplified Townsend model adapted from [4], which includes the species e, I^+, and I^-. Swarm parameters (mobility, diffusivity and ionization and attachment coefficients) are extracted from a lookup table generated by the Boltzmann solver LoKI-B [5], as a function of the reduced electric field. Ion mobility values are taken from [6]. The second kinetic scheme, proposed by Parent et al. [6], considers six species (e, N_2, O_2, $N_2{}^+$, $O_2{}^+$, and $O_2{}^-$) involved in thirteen reactions. The third scheme, from [7], extends this to nine species by including N, O, and $O_4{}^+$, for a total of twenty-six reactions. For both the six- and nine-species models, mobilities are taken from [6] and [8], respectively, and diffusivities are computed using the Einstein relation. For the electrostatic problem, Dirichlet boundary conditions are applied at both the emitter and the collector. Additionally, a set of boundary conditions from [9] is applied to the particle fluxes, as shown in the following table:

species	emitter	collector
e	$\Gamma \cdot \hat{n} = n(v_{th}/2 + \mathbf{U})$	$\Gamma \cdot \hat{n} = n(v_{th}/2) - 2\Gamma^+\gamma$
I^+	$\Gamma \cdot \hat{n} = n(v_{th}/2)$	$\Gamma \cdot \hat{n} = n(v_{th}/2 + \mathbf{U})$
I^-	$\Gamma \cdot \hat{n} = n(v_{th}/2 + \mathbf{U})$	$\Gamma \cdot \hat{n} = n(v_{th}/2)$

Table 1: Boundary condition for the *drift-diffusion* problem

Γ^+ is the sum of all positive ion fluxes, $\gamma = 0.01$ is the secondary emission coefficient, v_{th} is the thermal velocity and $\mathbf{U}$ is the drift velocity. The condition $\Gamma \cdot \hat{n} = 0$ is imposed for all neutrals.

Experimental set-up

A concentric wire-cylinder reactor, shown in Fig. 1, was constructed to experimentally validate the model. The wire had a curvature radius of $50\,\mu$m, and the surrounding cylinder had a radius of 3.75 cm. A high-voltage generator was connected to the emitter, while a pressure sensor monitored the internal pressure of the reactor. In addition, a comprehensive voltage-current measurement campaign was conducted over a wide voltage range.

Simulation results

Simulations were performed using the same geometry as the experimental set-up at atmospheric pressure to compare the I-V curve from the numerical model with the experiments.

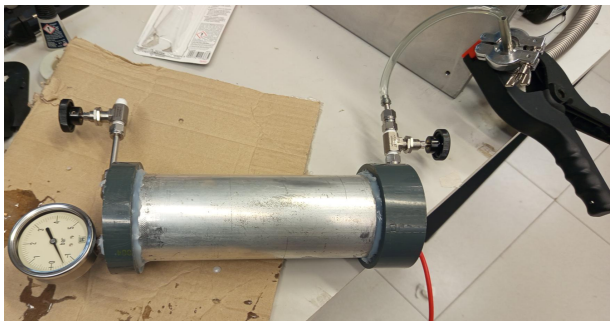

Figure 1: Concentric wire-cylinder reactor used for DC corona discharge experiments.

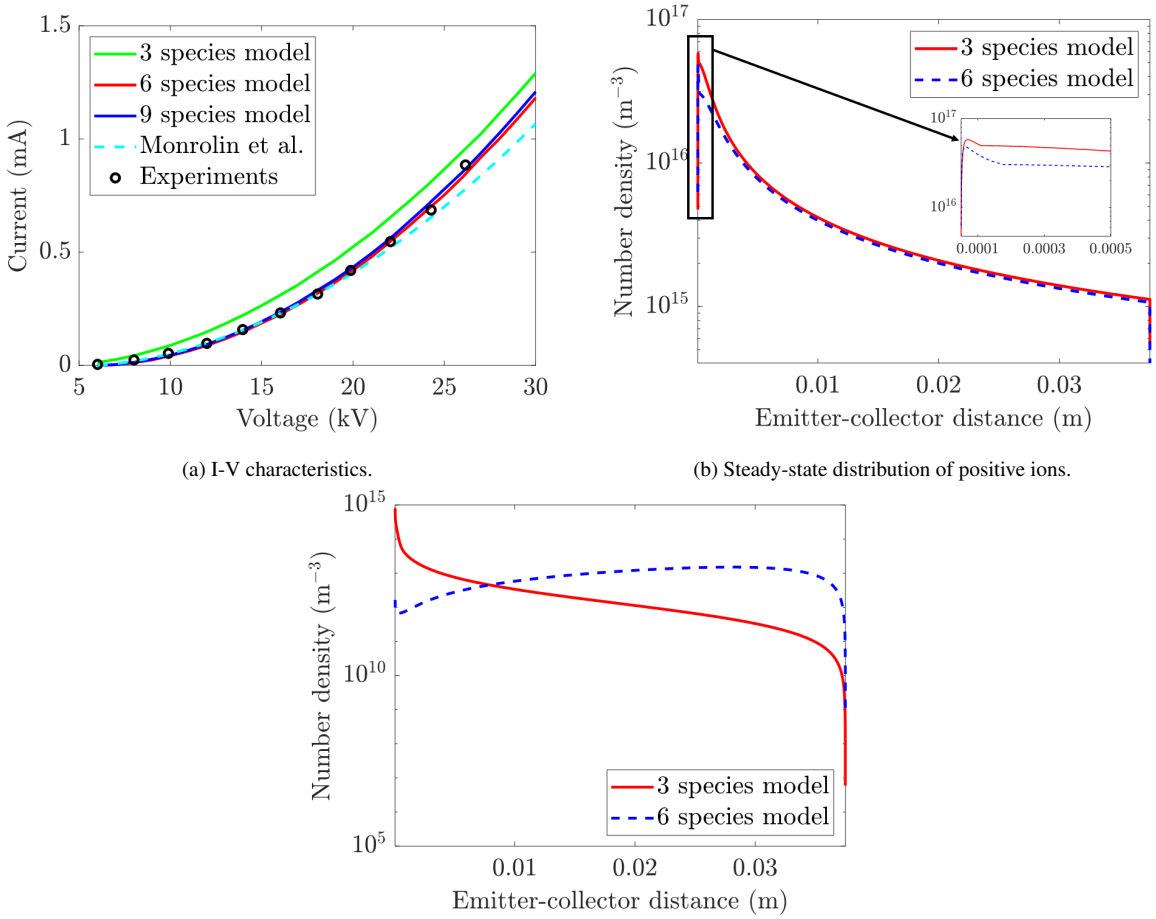

(a) I-V characteristics.

(b) Steady-state distribution of positive ions.

(c) Steady-state distribution of negative ions.

Figure 2: I-V characteristics and ion density profiles from numerical models.

Fig. 2a shows a comparison between the simulation results, experimental data, and the analytical model proposed in [10]. The discharge current is calculated using the generalized version of Sato's equation [3]. Even though the three employed reaction schemes are much simpler than extensive models suitable for 0D simulations [11], simulation results are in good agreement with the experimental data and the analytical model over a wide voltage range. In particular, the error between the curve obtained from the *drift-diffusion* model using the six- and nine-species mod-

els and the experimental data is minimal. On the other hand, the three-species model predicts higher currents. Figs. 2b and 2c show the steady-state distribution of positive and negative ions, respectively, obtained using the three-species and six-species models (in this one is considered the sum of O_2^+ and N_2^+). The distribution of positive ions predicted by both models is similar across the entire domain, while the distribution of negative ions differs. The three-species model predicts a lower concentration of negative ions in the drift region and a higher concentration in the ionization region. Furthermore, the curve predicted by the six-species model shows an increase in the drift region. This difference arises not only from the attachment reaction rates, which increase as the electric field decreases, but also from a significantly stronger recombination effect in the six-species model.

Conclusions

The obtained results demonstrate the significant impact of the choice of reaction scheme on the simulations. In particular, the I-V curves predicted by the more comprehensive models closely match the experimental data, while the three-species model predicts higher currents. Additionally, the behavior of negative ions differs between the models. Future research will focus on studying the discharge behavior at lower pressure levels to investigate how an ionic wind device operates at varying altitudes.

Acknowledgements

Funded by European Union

Funded by the European Union Grant Agreement No 101098900. Views and opinions expressed are however those of the author(s) only and do not necessarily reflect those of the European Union or EISMEA. Neither the European Union nor the granting authority can be held responsible for them.

References

[1] A. Popoli et al., Journal of Propulsion and Power, **41(1)** 40-52 (2025), 10.2514/1.B39268

[2] S. Trovato et al., J. Phys. D: Appl. Phys., **58** 015201 (2025), 10.1088/1361-6463/ad7d9c

[3] F. Ragazzi et al., IEEE Access, **12** 12545-12561 (2024), 10.1109/ACCESS.2024.3356865.

[4] R. Morrow et al., J. Phys. D: Appl. Phys., **30** 614 (1997), 10.1088/0022-3727/30/4/017

[5] A. Tejero-del-Caz et al., Plasma Sources Science and Technology, **28(4)** 043001 (2019), 10.1088/1361-6595/ab0537

[6] B. Parent et al., Journal of Computational Physics, **51-69**, 259 (2014), 10.1016/j.jcp.2013.11.029

[7] V.Y. Kozhevnikov et al., Energies, **16**, 4861 (2023), 10.3390/en16134861

[8] Y. Sakiyama et al., J. Phys. D: Appl. Phys., **45** 425201 (2012), 10.1088/0022-3727/45/42/425201

[9] V.V. Gorin et al., Phys. Plasmas, **27** 013505 (2020), 10.1063/1.5120613

[10] N. Monrolin et al., Phys Plasmas, **25 (6)** 063503 (2018), 10.1063/1.5031780

[11] G. Pierotti et al., Plasma Chem Plasma Process, **44** 1575–1594 (2024), 10.1007/s11090-024-10484-6